Distal connectivity causes summation and division across mouse visual cortex

Tatsuo K Sato[1], Michael Häusser[2] & Matteo Carandini[1]

Neurons in different locations across the cortex are connected through polysynaptic networks involving both excitation and inhibition. To probe the functional effect of such networks, we used optogenetic stimulation to trigger antidromic spikes in a local region of primary visual cortex (V1). This local activity had two effects at distal V1 locations: summation and division. The balance between the two depended on visual contrast, and a normalization model precisely captured these effects.

Neurons in primary visual cortex (V1) receive cortical input not only from neighboring neurons, but also from networks of distal intracortical connectivity[1]: horizontal connections in area V1 (refs. 2–4) and feedback connections from higher visual areas[5]. These networks are generally polysynaptic and target both excitatory and inhibitory neurons[6–10]. It is not known whether their overall functional effect is activation or suppression and whether this effect is fixed or depends on other factors. To answer these questions, we measured the causal effect of connectivity across mouse visual cortex in multiple visual contexts.

To evoke spikes reliably and focally in a local region, we developed an approach based on antidromic optogenetic stimulation *in vivo* (**Fig. 1**). This method builds on previous studies using optogenetic axonal stimulation *in vitro*[11] and *in vivo*[12]. Using *in utero* electroporation, we expressed Channelrhodopsin-2 (ChR2)-Venus in pyramidal neurons of one hemisphere[9,11] (**Fig. 1a**), obtaining strong expression in layer 2/3 (**Fig. 1e**). We then stimulated the callosal neurons in the binocular zone[13] using laser pulses targeted to their axon terminals in the contralateral hemisphere (**Fig. 1d,f**). Contralateral laser stimulation reliably elicited spikes in the binocular zone, first in layer 2/3 and then in layer 5 (**Fig. 1g** and **Supplementary Fig. 1**). Ionotropic glutamate receptor (iGluR) blockers abolished all spikes in the deeper layers, but not in the superficial layers, confirming that the latter are antidromic (**Fig. 1h** and **Supplementary Fig. 1**).

The strong early activity evoked locally in the callosal region was often accompanied by weaker, delayed activity in distal V1 sites in the monocular zone (**Fig. 2a–c** and **Supplementary Fig. 2**). When measured with local field potentials, this distal activation was stronger and more transient than the activation caused by visual stimuli placed on the vertical meridian; the latter, moreover, was not effective at producing spikes (**Supplementary Fig. 3**).

We next repeated these experiments in the presence of increasing visual contrast and found that the effect of distal intracortical connectivity changed from activation to progressively stronger suppression (**Fig. 2d–m**). For example, a site in the monocular zone that showed clear activation in the absence of visual stimuli (0% contrast; **Fig. 2a**) showed suppression when its activity was elevated with a stimulus of 25% or 50% contrast (**Fig. 2d,g,j**). These effects were common across sites (**Fig. 2b,e,h,k**), and even sites that showed no activation showed robust suppression (**Fig. 2c,f,i,l** and **Supplementary Table 1**). Overall, the population of neurons showed a gradual transition from activation to suppression in the presence of increasing contrast (**Fig. 2m** and **Supplementary Fig. 4**). These effects were seen not only in multiunit activity, but also in well-isolated neurons (**Supplementary Fig. 5**).

Activation and suppression exhibited different spatial footprints. Although activation could be seen at all locations (first in the binocular zone and later in the monocular zone, with decreased amplitude), suppression was present only in the monocular zone, particularly in the far monocular zone (**Supplementary Fig. 6**). Suppression, in other words, appeared only in regions that were directly driven by visual stimuli. Moreover, it appeared only when those stimuli had high contrast. This was not solely a result of the higher baseline firing rates: suppression was absent in the visual responses to a bar flashed after optogenetic stimulation (**Supplementary Fig. 7**).

To summarize these contrast-dependent effects of distal intracortical connectivity, we employed the model of divisive normalization[14]. In the model, the responses in the far monocular zone depend on local contrast c as

$$R(c) = \frac{c^n + p\lambda}{c_{50}^n + c^n + q\lambda} \qquad (1)$$

where c_{50} and n control responsiveness to local contrast, λ indicates the strength of the distal optogenetic stimulation, and p and q determine the degree to which the distal site provides activation and suppression.

The model provided good fits to the data, capturing the dependence of the responses on local contrast (**Fig. 3a,b**) and accounting for $96.4 \pm 2.9\%$ ($n = 103$) of the variance for the individual sites. At sites showing activation, it captured how increasing contrast changed the effect of the optogenetic stimulus from activation to suppression (**Fig. 3a**). At sites showing only suppression, the model correctly described how suppression effectively scaled the contrast of the visual stimulus, stretching the contrast response curve divisively on the abscissa (**Fig. 3b**). The two groups of sites shared the same denominator: the only parameter that varied across them was the activation factor p, which was zero in the sites that did not show activation (**Fig. 3b**).

The normalization model also predicted the effects of changes in the strength of optogenetic stimulation (**Fig. 3c,d**). Reducing laser power had similar effects on activation and on suppression: it reduced both (**Fig. 3c** and **Supplementary Fig. 8**). The model provided good

[1]UCL Institute of Ophthalmology, University College London, London, UK. [2]Wolfson Institute for Biomedical Research and Department of Neuroscience, Physiology and Pharmacology, University College London, London, UK. Correspondence should be addressed to T.K.S. (t.sato@ucl.ac.uk).

Figure 1 Optogenetic antidromic stimulation for probing cortical connectivity in V1. (**a**) The targets of optogenetic stimulation are layer 2/3 (L2/3) neurons in the callosal binocular zone (BZ) in the electroporated hemisphere. MZ, monocular zone. (**b**) Top view of the chamber allowing access to both hemispheres. Rectangles indicate regions shown in **c**. (**c**) Retinotopic maps obtained via intrinsic imaging. V1 and lateromedial area were determined on the basis of reversal of retinotopy. Curves indicate representation of the vertical meridian (dotted) and horizontal meridian (dashed). (**d**) Fluorescence image showing expression of ChR2-Venus. Rectangle indicates the callosal band, processed separately to enhance signals. Curves are replotted from **c**. Scale bar also applies to the images in **b**. (**e**,**f**) Coronal sections of electroporated (**e**) and contralateral (**f**) hemispheres. (**g**) Response histograms for two units in putative L2/3 (top) and one in putative L5 (bottom). Inset, spike shapes of the two units. (**h**) Data are presented as in **g** in the presence of iGluR blockers (CNQX and D-AP5).
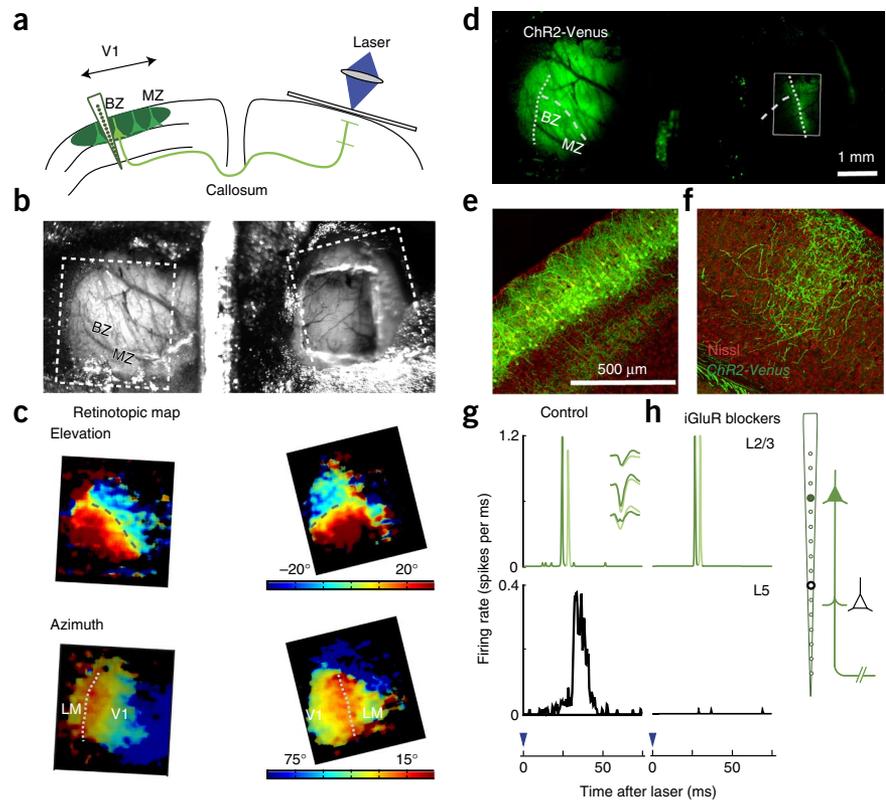

fits to these data, explaining 93.8% of the variance and capturing the effect of laser intensity with a single parameter, λ (which was set to 0, 0.54 and 1 for laser powers of 0, 25 and 100 mW, respectively).

These results indicate that the causal, functional effect of distal intracortical connectivity depends on the strength of sensory stimulation in the destination region. If this region is driven weakly, the effect is arithmetical summation. If this region is instead driven strongly, the effect is arithmetical division. For intermediate levels of drive, both effects are present. The exact strength of each is described by a simple normalization equation.

Our findings may provide a basis for understanding how the responses of V1 neurons are shaped by lateral interactions across the visual field and how these interactions depend on visual context[14–20]. Indeed, many of these interactions can be described by a similar normalization model[14]. Previous experiments, however, involved recording at one location in V1 while presenting stimuli at local and distal positions in the visual field. As such, these experiments could not clamp distal activity at a given level, and could not directly assess the causal role of this activity in eliciting activation or suppression.

Figure 2 Contrast dependence of effects of distal activation. Electrodes were placed in the far monocular zone and neurons there were stimulated with white-noise visual stimuli. (**a**–**c**) Firing rate responses of three units in the far monocular zone (receptive field center = 85°, 55° and 75°) to antidromic stimulation of the binocular zone (solid curves), in the absence of visual stimulation (0% contrast). Dashed curves indicate activity in the control condition. In the first two units, distal stimulation caused activation. Inset, experimental schematic. (**d**–**f**) Data presented as in **a**–**c** in the presence of visual contrast (25, 50 and 25% contrast). In all of the units, the effect of distal stimulation became suppressive. In the second unit, suppression coexisted with activation. (**g**–**i**) Data presented as in **a**–**c** at higher contrast (50, 100 and 50%). In all units, the effect of distal stimulation was purely suppressive. Blue arrowhead indicates laser pulse time (0 ms). (**j**–**l**) Summary of the results for the three units, plotted as the difference in firing rate between control and laser conditions. (**m**) Summary of the results for all sites. Responses were averaged between 50 and 250 ms after laser onset, in the absence (control) and presence (laser) of distal activation. Red bars represent sites with activation and suppression (n = 56) and blue bars represent sites with suppression alone (n = 47).
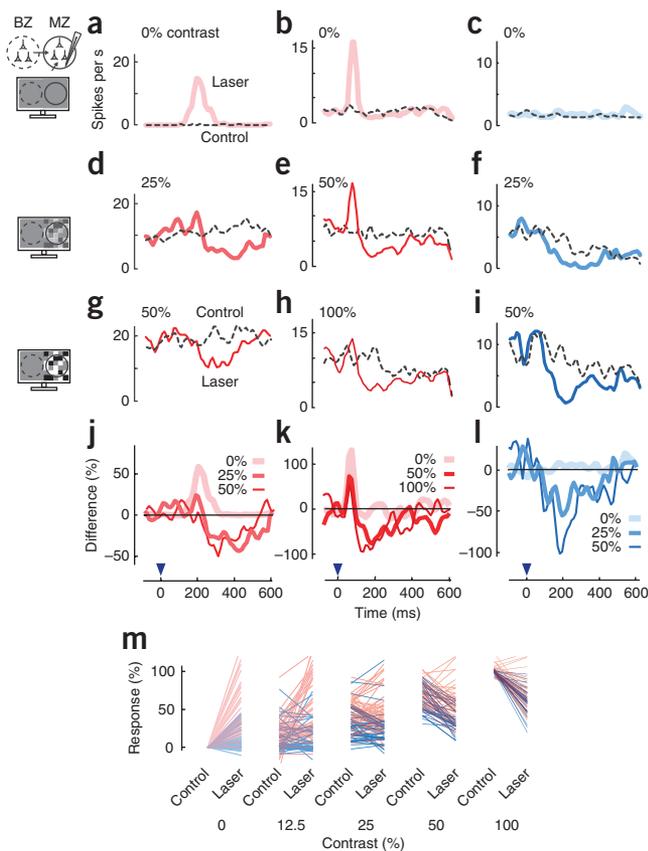
Figure 3 Normalization summarizes the effects of distal activation. (**a**) Population response as a function of stimulus contrast for sites showing activation at zero contrast. (**b**) Data presented as in **a** for sites showing only suppression. Curves indicate the fit of the normalization model (equation (1)). (**c**) Effects of changing laser power for sites showing activation at zero contrast. (**d**) Data presented as in **c** for the remaining sites. Error bars represent ±median absolute deviation.

We used a new strategy to probe cortical function using antidromic optogenetic stimulation. This strategy presents fundamental advantages when investigating circuits with reciprocal connectivity: it imposes a level of activity in a local region regardless of the reciprocal inputs that it receives from distal regions. Moreover, because the antidromic stimulus is optogenetic, it is not corrupted by orthodromic effects.

We paired antidromic optogenetic stimulation with visual stimulation and with recordings at multiple V1 sites. This combination of techniques allowed us to characterize the causal and functional effects and the arithmetical properties of distal intracortical connectivity. Further research is required to understand the cellular and circuit mechanisms underlying these causal effects, and the behavioral advantages of these computations. Our method of antidromic optogenetic stimulation could be useful for enabling such further advances.

METHODS

Methods and any associated references are available in the online version of the paper.

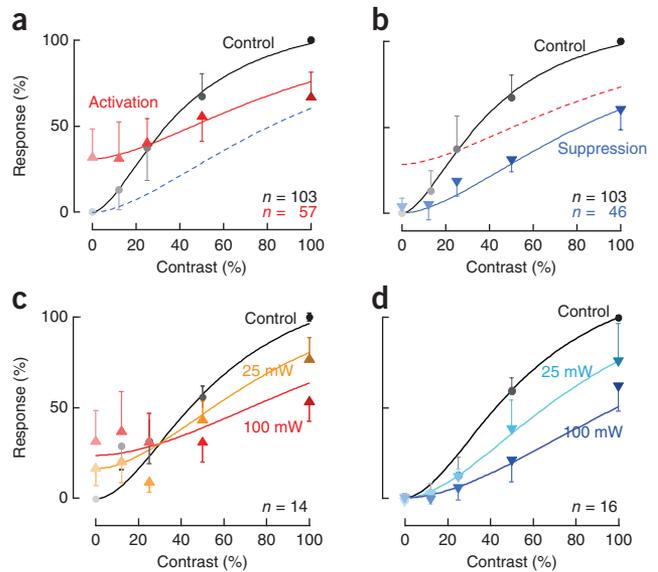*Note: Any Supplementary Information and Source Data files are available in the online version of the paper.*

AUTHOR CONTRIBUTIONS
T.K.S., M.H. and M.C. designed the study. T.K.S. performed the experiments. T.K.S. and M.C. analyzed the data. T.K.S., M.H. and M.C. wrote the paper.

COMPETING FINANCIAL INTERESTS
The authors declare no competing financial interests.

Reprints and permissions information is available online at http://www.nature.com/reprints/index.html.

1. Schüz, A., Chaimow, D., Liewald, D. & Dortenman, M. *Cereb. Cortex* **16**, 1474–1486 (2006).
2. Gilbert, C.D. & Wiesel, T.N. *J. Neurosci.* **9**, 2432–2442 (1989).
3. Bosking, W.H., Zhang, Y., Schofield, B. & Fitzpatrick, D. *J. Neurosci.* **17**, 2112–2127 (1997).
4. Adesnik, H., Bruns, W., Taniguchi, H., Huang, Z.J. & Scanziani, M. *Nature* **490**, 226–231 (2012).
5. Angelucci, A. & Bressloff, P.C. *Prog. Brain Res.* **154**, 93–120 (2006).
6. McGuire, B.A., Gilbert, C.D., Rivlin, P.K. & Wiesel, T.N. *J. Comp. Neurol.* **305**, 370–392 (1991).
7. Anderson, J.C. & Martin, K.A. *J. Neurosci.* **29**, 11283–11293 (2009).
8. Hirsch, J.A. & Gilbert, C.D. *J. Neurosci.* **11**, 1800–1809 (1991).
9. Adesnik, H. & Scanziani, M. *Nature* **464**, 1155–1160 (2010).
10. Dong, H., Shao, Z., Nerbonne, J.M. & Burkhalter, A. *J. Comp. Neurol.* **475**, 361–373 (2004).
11. Petreanu, L., Huber, D., Sobczyk, A. & Svoboda, K. *Nat. Neurosci.* **10**, 663–668 (2007).
12. Lee, J.H. *et al. Nature* **465**, 788–792 (2010).
13. Olavarria, J.F. & Hiroi, R. *J. Comp. Neurol.* **459**, 156–172 (2003).
14. Carandini, M. & Heeger, D.J. *Nat. Rev. Neurosci.* **13**, 51–62 (2011).
15. Levitt, J.B. & Lund, J.S. *Nature* **387**, 73–76 (1997).
16. Sceniak, M.P., Ringach, D.L., Hawken, M.J. & Shapley, R. *Nat. Neurosci.* **2**, 733–739 (1999).
17. Nauhaus, I., Busse, L., Carandini, M. & Ringach, D.L. *Nat. Neurosci.* **12**, 70–76 (2009).
18. Kapadia, M.K., Westheimer, G. & Gilbert, C.D. *Proc. Natl. Acad. Sci. USA* **96**, 12073–12078 (1999).
19. Somers, D.C. *et al. Cereb. Cortex* **8**, 204–217 (1998).
20. Polat, U., Mizobe, K., Pettet, M.W., Kasamatsu, T. & Norcia, A.M. *Nature* **391**, 580–584 (1998).

ONLINE METHODS

Approval for experiments with animals. Experiments were conducted according to the UK Animals (Scientific Procedures) Act 1986 under personal and project licenses issued by the Home Office following ethical review.

In utero electroporation. In utero electroporation was performed as described previously[21,22]. Embryonic day 15.5 timed-pregnant C57BL/6 mice (Harlan) were anesthetized with 2% isoflurane in oxygen. Up to 1 μl of DNA solution with Fast Green (Sigma) was pressure-injected into one lateral ventricle of embryos. The solution[9,11,23] contained pCAGGS-ChR2-Venus (Addgene 15753, 1.5 μg μl^{-1}) and pCAG-mCherry (0.5 μg μl^{-1}). Electroporation was achieved with 5 square pulses (50 V, 50 ms, 1 Hz, CUY21, NepaGene). We used mCherry fluorescence to screen for positive animals at postnatal day 0. Mice were maintained with a light-dark cycle of 12:12 h, and up to four mice were kept in one cage after weaning.

Surgery. Electroporated mice (n = 19, both sexes, 1–2 month old) were anesthetized and prepared for experiments that commonly lasted 8–10 h. For initial surgery (30–60 min), anesthesia was obtained with ketamine and xylazine. After a tracheotomy, mice were placed in a stereotaxic frame, and anesthesia was switched to 2% isoflurane. Temperature was maintained at 37 °C using a feedback-controlled heating pad (TR-200, FST). Carprofen (10 mg per kg of body weight), atropine (0.3 mg per kg) and dexamethasone (2 mg per kg) were applied to prevent pain, secretions and brain edema. Eyes were covered with contact lenses (Pmma 003, Veterinary Specialty Products). The eyelids of the unstimulated eye were sutured. A head-plate was implanted to the skull with black dental cement (Ortho-Jet powder, Lang Dental). A cranial window was embedded at the callosal stimulation side (**Fig. 1b**). Only mice showing a clear Venus-labeled callosal band (**Fig. 1d**)[22] were used for subsequent measurements.

Intrinsic imaging. In every mouse, we obtained retinotopic maps for elevation and azimuth (**Fig. 1c**) to identify the location of V1 in both hemispheres (**Fig. 1c**). Optical images were obtained using a CMOS camera (MV-D1024E-CL, PhotonFocus) controlled by custom software. We imaged the surface vascular pattern with green light (525 nm) and obtained intrinsic signal images with red light (625 nm, LEDC_HB02-G-R, Doric). Images were acquired at 10-Hz frame rate. The intrinsic signal was analyzed for 5 s after the onset of 4-s-long visual stimuli.

Electrophysiology. Having identified the position of V1, we performed a craniotomy (usually 500 × 500 μm, 500 × 1,750 μm for a multi-shank electrode) and a durotomy (for multi-shank electrodes), and covered the brain with 1% agarose. Anesthesia was then continued at a lower concentration of isoflurane (0.125–0.5%), supplemented with chlorprothixene (1 mg per kg, Sigma). A multichannel silicon probe mounted on a micromanipulator (Junior, Luigs & Neumann) was slowly advanced into the brain (depth = 700–900 μm), and recording started 20 min after the insertion. Insertion was targeted to a retinotopic area with ~20° elevation (the center of an LCD monitor) and azimuth of 0–90° within V1, based on retinotopic maps (**Fig. 1d**). Voltage signals were amplified and digitized at 30 kHz (Cerebus, Blackrock Microsystems). Probes had a single shank (A1x16-5mm-50-703, A1x32-Edge-5mm-50-177, NeuroNexus) or multiple shanks (A2x16-5mm-50-413, A4x8-5mm-50-400-413). With single-shank probes, insertion was occasionally performed twice in the same preparation.

For blockade of iGluRs, we applied a mixture of CNQX and D-AP5 (2 mM in HEPES-buffered artificial cerebrospinal fluid, Tocris) to the dura surface without agarose. Pharmacological effects were evaluated at least 15 min after application.

Optogenetic stimulation. To stimulate callosal terminals optogenetically, we used a blue laser (MBL-III-473nm-150mW, CNI). The laser was directed into an optical fiber (200-μm diameter), and laser output from the fiber was refocused onto callosal band with two convex lenses (f1/f2 = 0.33) at an incident angle of 30°, as an ellipse (666 μm in mediolateral axis, 770 μm in anteroposterior axis). Vertical retinotopic positions of recording and stimulating sites were aligned. Callosal neurons sending projections to the binocular zone of contralateral V1 are the target of this stimulation, and they are known to lie in the binocular zone[24], mostly in V1 (ref. 13).

We set the laser power at the focus point to 100 mW, providing ~250 mW mm^{-2} at the dura surface. This intensity attenuates by half within 100 μm inside

cortical tissue[25]. We estimated from a previous report[23] that this intensity would activate <70% of ChR2-expressing axons. This intensity is reported to cause no damage even with illumination lasting 1 s (ref. 26) or 30 s (ref. 27). Laser illumination lasted 2 ms and was controlled with a high-speed shutter (LS3T2, Uniblitz). A small fraction of laser output was monitored with a photodiode (PDA100A, Thorlabs). The interstimulus interval was >3 s. In two mice, we also tested the effect of lower laser power (25 mW; **Fig. 3c,d** and **Supplementary Fig. 8**), using an ND filter (OD 0.6) mounted on a motorized wheel (FW103, Thorlabs).

Visual stimulation. Visual stimuli were presented on an LCD monitor (E2607WS, Iiyama, mean luminance = 50 cd m^{-2}, refresh rate = 75 Hz, gamma corrected), covering an angle of 100° horizontal and 65° vertical in the visual hemifield contralateral to the imaging or recording side.

For intrinsic imaging, flickering vertical black and white bars (spatial frequency 0.05 cycles per degree, temporal frequency = 2 Hz, 100% contrast, duration = 4 s) were presented at various azimuths, to obtain a horizontal retinotopic map. For a vertical map, we used horizontal bars.

For electrophysiology, we first presented a contrast-reversing square checkerboard (0.03 cpd, 2 Hz, 100%, 2 s) to identify the depth of presumed layer 4 (ref. 28). We then presented flickering vertical or horizontal bars (0.06 cpd, 1 Hz, 100%, 1 s) to measure retinotopic tuning at the recording site (**Supplementary Fig. 2b**). We then presented dynamic white noise (bright and dark 6° sized-squares, 10.7 frames per s, 1.6 s) covering the far monocular visual field (55–95° azimuth; **Fig. 2**). The random noise was different across blocks, but the same within blocks. There were at least 50 blocks, and each block involved 6–15 conditions in random order, the combination of 3–5 contrasts (0, 12, 25, 50 or 100%) and laser stimulation (0, 25 or 100 mW). The laser was activated 1 s after the noise onset.

Histology. After a terminal dose of ketamine/xylazine, mice (n = 3) were perfused with phosphate-buffered saline, followed by 4% formalhyde (wt/vol) in phosphate-buffered saline. Brains were harvested and placed in 30% sucrose solution (wt/vol) for 24 h. Coronal brain sections of 40 μm were cut using a cyrostat (CM1850, Leica), stained with Fluorescent Nissl (Invitrogen), and mounted in DAPI-containing Vectashield (Vector Labs). Confocal microscopy was performed on LSM 710 (Zeiss).

Data analysis. Data were analyzed in MATLAB (MathWorks). After bandpass filtering between 0.25–7.5 kHz, unit activity was extracted off-line using a template-matching algorithm based on a mean square distance metric[17]. This approach does not distinguish single neurons and multiunit activity, and so we also performed detailed spike-sorting based on principal component analysis on one data set (**Supplementary Fig. 5**). The spike sorting algorithm, MaskedKlustaKwik, is an improvement of KlustaKwik designed for dense electrode arrays (Kadir, S.N., Goodman, D.F.M., Schulman, J., Buzsaki, G. & Harris, K.D., *Soc. Neurosci. Abstr.* **680.08**, 2012).

We pooled responses across neurons by considering the multiunit activity at each electrode site. We classified our units on the basis of their retinotopic preferences, which could lie on the callosal zone (0–15°)[24], the acallosal zone (>15°), the binocular zone (0–30°)[29] and the monocular zone (>30°). Firing rates were obtained at 12.5-ms resolution by smoothing spike trains with a Gaussian window (σ = 12.5 ms). In the callosal binocular zone, a higher resolution was also used (125 μs) to characterize the layer differences (**Fig. 2e**).

Local field potentials (LFPs) were low pass-filtered at 2 kHz. To obtain current source density (CSD) profiles[30], we first subtracted a baseline component of LFP for each channel using the 50-ms period before the laser stimulation or flickering checkerboard visual stimulation. We then duplicated the uppermost and lowermost LFP traces and calculated the second derivative along the depth axis. To generate color images of CSD, we also performed linear interpolation along the depth axis and Gaussian-smoothing. The cortical depth of presumed L4 was determined from the responses to flickering checkerboards as the earliest CSD sink or the earliest negative LFP deflection[28]. Units above the presumed L4 were classified as superficial, and those below as deep.

To evaluate the effect of callosal laser stimulation on each unit, we considered the spike count per 25-ms bin over a range of 0–600 ms after laser onset time. For each block and each visual contrast presented, we made pairwise comparisons

of spike count between the conditions with and without laser stimulation (Wilcoxon signed rank test with Bonferroni correction, $P < 0.05$). For suppressive effects, we used 50-ms bin width because of the slower time course. We measured the effect of distal intracortical connectivity as the difference in firing rate between control condition and laser condition (**Fig. 2** and **Supplementary Figs. 4–6**). We normalized the difference curves in the far monocular zone (**Fig. 3e–j**), by dividing by the r_{100} of the fitted contrast-response curve (see below).

Statistical analysis. All the statistical tests were non-parametric, and indicated in the main text or figure legend. Our sample size was always larger than the minimum size that can yield $P < 0.05$ for each test. Data and bar plots were shown as median ± median absolute deviation, as they are robust to outliers.

Model fits. For units in the far monocular zone, we considered the firing rate 50–250 ms after laser onset time, when a maximal change could be expected (**Fig. 2m** and **Supplementary Fig. 6a**). We first fit the firing rate of the control condition (no laser) with a hyperbolic ratio function[11]

$$r(c) = r_0 + r_{max} \frac{c^n}{c_{50}^n + c^n}$$

where r_0 is the baseline firing rate, r_{max} is the maximum rate, c_{50} is the semisaturation contrast, and n is a constant determining the slope of the function. The values of r_0 and r_{100} were then used to normalize each unit's response to values R ranging from 0 to 1. We then fitted the control responses together with the responses measured with laser stimulation using the full normalization equation[11]

(Equation (1)). We imposed the same c_{50} and n, and obtained parameters p and q. To fit the population curves in **Figure 3a,b**, we fit the three curves simultaneously. For response with different laser power (0, 25 and 100 mW; **Fig. 3c,d**), we imposed the same c_{50}, n, p and q, while allowing for changes in λ (0 for control, 1 for 100 mW, and intermediate for 25 mW).

Model parameters were obtained by weighted least-squares fit, and fit quality was assessed by the percentage of variance in the responses R explained by the model predictions m

$$v = 1 - \frac{\sum_{i=1}^{n}(R_i - m_i)^2}{\sum_{i=1}^{n}(R_i - \bar{R})^2}$$

where the indices i indicate one of visual contrasts and $\bar{R}$ is the mean of the responses.

21. Saito, T. & Nakatsuji, N. *Dev. Biol.* **240**, 237–246 (2001).
22. Mizuno, H., Hirano, T. & Tagawa, Y. *J. Neurosci.* **27**, 6760–6770 (2007).
23. Huber, D. *et al. Nature* **451**, 61–64 (2008).
24. Wang, Q. & Burkhalter, A. *J. Comp. Neurol.* **502**, 339–357 (2007).
25. Aravanis, A.M. *et al. J. Neural Eng.* **4**, S143–S156 (2007).
26. Diester, I. *et al. Nat. Neurosci.* **14**, 387–397 (2011).
27. Anikeeva, P. *et al. Nat. Neurosci.* **15**, 163–170 (2011).
28. Niell, C.M. & Stryker, M.P. *J. Neurosci.* **28**, 7520–7536 (2008).
29. Wagor, E., Mangini, N.J. & Pearlman, A.L. *J. Comp. Neurol.* **193**, 187–202 (1980).
30. Bereshpolova, Y., Amitai, Y., Gusev, A.G., Stoelzel, C.R. & Swadlow, H.A. *J. Neurosci.* **27**, 9392–9399 (2007).